引用格式：XIAO Tong, TIAN Changhui, XU Cuilian, et al. Integrated Design of Optically Transparent Composite for Low Infrared Emission and Wideband Microwave Absorption Metasurface[J]. Acta Photonica Sinica, 2022, 51(1):0151117
肖桐,田昌会,徐翠莲,等.一体化光学透明红外与雷达兼容隐身复合超表面[J].光子学报,2022,51(1):0151117

一体化光学透明红外与雷达兼容隐身复合超表面

肖桐,田昌会,徐翠莲,高志强
(空军工程大学 基础部,西安 710051)

摘　要:基于可见光透明材料氧化铟锡(ITO)、聚对苯二甲酸乙二醇酯(PET)以及聚甲基丙烯酸甲酯(PMMA),采用红外低发射层和雷达吸波层一体化设计的思路,实现了光学透明的红外-雷达兼容隐身复合超表面。该结构由功能层、介质层以及反射背板三部分组成,总厚度仅有1.17 mm。通过在功能层表面蚀刻出ITO图案并优化图案尺寸实现了微波波段15.9~35.1 GHz频带范围内高于90%的宽带吸收。同时利用提高功能层表面ITO占空比的方法降低了红外波段的发射率,结构表面红外发射率控制在0.25左右。该结构厚度较薄,同时具备较好的宽频带雷达吸波性能、低红外发射率以及可见光透明特性。

关键词:红外-雷达兼容隐身;红外低发射;雷达吸波;超表面;光学透明
中图分类号:TB34　　**文献标识码**:A　　**doi**:10.3788/gzxb20225101.0151117

0　引言

随着战场环境的日益复杂和多频谱复合探测技术的发展,各种先进的探测手段以及探测设备对现有装备的生存构成了严重威胁。因此常规的单一波段隐身能力已经难以满足现代战争的要求。针对目前主要的探测手段——红外探测和雷达探测,如何有效实现二者的兼容隐身是当前隐身材料技术中的研究热点[1-5]。

作为主动探测技术,雷达探测需要主动发射并接收雷达波,据回波信号的特征对目标进行发现、跟踪甚至截获。因此雷达隐身要求材料能够尽可能减少对雷达波的反射,目前“漫反射”和吸波是常用且有效的技术手段。与雷达探测不同的是,红外探测是被动探测,只依据目标自身的红外辐射进行探测,目标红外辐射特征越强就越容易被发现,因此对于红外隐身材料的核心要求就是减少红外辐射,而降低材料红外发射率是当前主流且有效的做法。根据基尔霍夫定律,低发射意味着低吸收同时也意味着高反射,这一点与雷达隐身所要求的低反射是矛盾的。如何有效地解决这一矛盾是红外-雷达兼容隐身的核心所在[6-8]。当前,研究者们在这一领域已做出了一些有效的尝试。一些研究者提出把氧化锌(ZnO)、三氧化二铟(In_2O_3)等半导体材料粉碎后和树脂、漆等基料进行混合形成复合涂料,以期通过调节掺杂半导体的粒度和涂层厚度来调节雷达波和红外辐射的反射和吸收[9-11]。但是,受限于红外和雷达隐身对于材料要求的矛盾,想要在提升雷达吸波能力的同时降低红外发射率是非常困难的。也有一些研究者提出利用光子晶体实现兼容隐身的目的[12-13]。光子晶体在抑制红外辐射、红外与激光以及可见光兼容隐身方面优势突出,但在雷达隐身方面具有一定的局限性[14-15]。

近年来,超材料在隐身技术中引起了很大关注。而超表面作为一种特殊的二维超材料,更适合于红外-

基金项目:国家自然科学基金(No.12004437),陕西省自然科学基础研究计划(No.2020JQ-471)
第一作者:肖桐(1993—),男,硕士研究生,主要研究方向为红外及多频谱兼容隐身技术。Email: xt415574621@163.com
导师(通讯作者):田昌会(1963—),男,教授,博士,主要研究方向为红外辐射特性及探测技术研究。Email:tchtyb001@163.com
收稿日期:2021-07-05;**录用日期**:2021-10-15

雷达兼容隐身结构的设计。例如，ZHANG C等提出了一种多层超表面结构，厚度为2.26 mm，可以实现8～16 GHz的宽带微波吸收，同时红外发射率控制在0.2[16]。TIAN Hao等设计了一种结构，吸波频段可以覆盖整个X波段，同时红外发射率小于0.3[1]。XU C给出了同时具有五个强微波吸收峰和低红外发射率的雷达红外隐身兼容结构[17]。但这些研究使用的都是不透明材料。此外，对于可见光透明超材料，也有研究报道。SHRESTHA S展示了一种可见光透明红外吸收体，其在4～16 μm范围内的吸收率大于80%[18]。ZHANG C等提出了一种光学透明的微波宽带吸收体，在8.3～17.4 GHz范围内吸收率大于90%[19]。这些研究虽然融合了可见光，但都没有实现可见光、红外和雷达的兼容隐身。目前，针对可见光透明的红外-雷达兼容隐身材料研究，基本思路都是在雷达吸波层上覆盖红外低发射层，该红外低发射层在微波频段具有较高的透射率。例如，MENG Z等提出一种可见光透明的多层复合超表面结构，可以实现11.2～33.9 GHz范围内宽带微波吸收，同时红外发射率控制在0.3[20]。徐翠莲等通过结构优化实现了更高带宽的微波吸收，同时兼顾了红外低发射率以及可见光透明[21]。这种设计思路利用可见光透明的两个功能层分别实现红外和雷达的隐身要求，具有方便调控的特点，但由于多层结构的设计，整体结构较为复杂且增加了材料厚度，使得光学透明效果有所下降。

本文利用透明导电氧化铟锡(ITO)材料，设计了一种红外-雷达兼容隐身超表面，将红外低发射层和雷达吸波层进行整体设计，厚度仅为1.17 mm。实现了微波波段15.9～35.1 GHz频带内吸收率高于90%的宽带吸波；通过提高吸波层表面ITO占比的方式实现了红外波段3.0～14.0 μm的低发射，平均发射率为0.25左右，并进一步研究了其光学透明特性。

1 结构设计与仿真实验

1.1 结构设计

为了满足光学透明的要求，整个结构所用材料均为光学透明材料。图1为单元结构的示意图。该结构顶层使用方阻为6.0 Ω/sq的ITO，并刻蚀出图1(b)所示的图案，ITO基底采用厚度为d_1的聚对苯二甲酸乙二醇酯(PET)。聚对苯二甲酸乙二醇酯作为一种可见光透明的材料，其介电常数为3.0(1－j0.06)。ITO是一种N型氧化物半导体材料，是氧化铟锡和铟氧化物的混合物。由于其具有接近金属的电阻率同时还有光学透明的特性，因此在液晶显示、光伏材料、建筑玻璃领域得到了广泛应用。近年来，随着武器装备光学透明窗口隐身需求的快速发展，低阻值的ITO薄膜所具有的红外低发射率特性受到了众多研究者的关注，因此在红外雷达兼容隐身领域有着巨大发展前景。ITO在可见光范围是透明的，在红外波段的介电常数满足Drude模型[22]

$$\varepsilon(\omega)=\varepsilon_{\mathrm{b}}-\frac{\omega_{\mathrm{p}}}{\omega\left(\omega+\mathrm{i}\omega_{\mathrm{c}}\right)} \tag{1}$$

式中，$\varepsilon_{\mathrm{b}}=3.9$；等离子体频率$\omega_{\mathrm{p}}=461$ THz；碰撞频率$\omega_{\mathrm{c}}=28.7$ THz。计算可得介电常数的实部为负，这表明ITO在红外波段的行为类似于金属。结构底部采用方阻为6.0 Ω/sq的整片ITO薄膜作为反射背板，顶层和底层中间使用厚度为d_2的聚甲基丙烯酸甲酯(PMMA)，其介电常数为2.25，损耗角正切值为0.001。结构顶层的图案由四种不同尺寸的方形贴片组成，分别为边长为a_2的中心正方形，边长为a_1的四个较大的正方形，边长为a_3的外围小正方形，以及四个长边为b_2，短边为b_1的长方形。优化后的尺寸为：$a_1=1.10$ mm，$a_2=0.30$ mm，$a_3=0.10$ mm，$b_1=0.20$ mm，$b_2=1.05$ mm，$d_1=0.17$ mm，$d_2=1.00$ mm。另外，方阻为6.0 Ω/sq的ITO薄膜厚度约为175 nm，该厚度由于工艺问题可能略有浮动，但由于和整体结构厚度相比量级很小，因此ITO薄膜层的厚度对整体试验没有影响。

根据该结构表面ITO和PET两种不同发射率材料的占空比，整体结构的总发射率可表示为[23]

$$\varepsilon=\varepsilon_{\mathrm{ITO}}f_{\mathrm{ITO}}+\varepsilon_{\mathrm{S}}f_{\mathrm{S}} \tag{2}$$

式中，ε是整个结构的发射率，$\varepsilon_{\mathrm{ITO}}$和$\varepsilon_{\mathrm{S}}$分别是ITO和用于ITO蚀刻的衬底材料即PET的发射率。f_{ITO}为ITO部分的占空比(ITO面积/总面积)，$f_{\mathrm{S}}=1-f_{\mathrm{ITO}}$，为衬底材料PET的占空比。片状电阻为6 Ω/sq的ITO的发射率在0.1左右，PET的发射率一般低于0.9。经过计算，该结构的红外发射率仅为0.25。

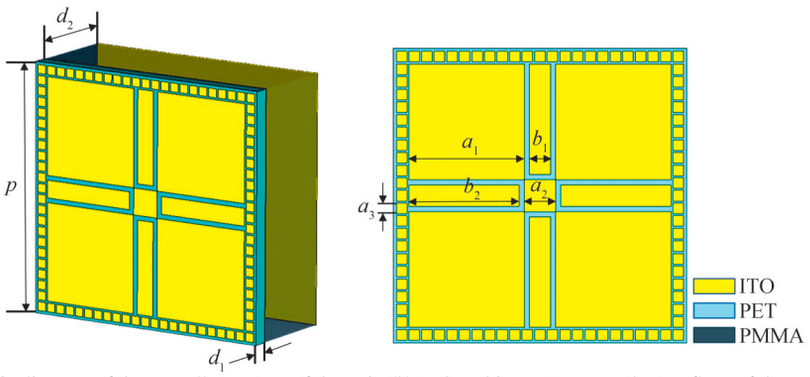

(a) Schematic diagram of the overall structure of the unit (b) ITO etching patterns on the top floor of the unit

图1 单元结构示意

Fig.1 Schematic diagram of the unit structure

1.2 仿真与分析

利用CST微波工作室软件对设计结构的吸收、反射和透射进行计算。x、y方向采用unit cell边界条件，$\pm z$方向分别设置两个激励端口，一个为发射端口，另一个为接收端口。图2为电磁波垂直入射时反射率、透射率和吸收率的仿真结果。从图中可以看出，由于ITO反射背板的存在，该结构的透射率几乎为0。反射率在15.9～35.1 GHz范围内低于10%，而吸收率通过$A=1-R=1-|S_{11}|^2$计算得到，其中$|S_{11}|^2$为反射率，该结构在15.9～35.1 GHz频带内实现了吸收率高于90%的宽带吸波。

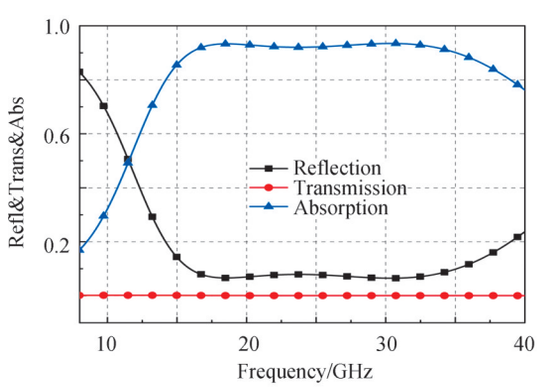

图2 吸收、反射以及透射率仿真结果

Fig.2 Simulation results of absorption, reflection and transmittance

图3为不同入射角下的吸收率。对于TE模式，在入射角小于30°时该结构能够保持较高的吸收率，随着角度进一步增大，低频部分的吸收率下降较多。对于TM模式，入射角较小时该结构吸收率只有0.8左右，而随着入射角增加至35°，该结构在20.1～35.0 GHz范围内能够保持90%的吸收率。说明该结构在TM模式下的大入射角吸波能力强于TE模式。这是由于入射面上磁场分量的变化引起的。对于TE模式，入射面的磁场分量可以表示为$H_{x-y}=H\cos\theta$，其中H是入射电磁波磁场强度，θ为入射角。可以看到随着入射角的不断增大，入射面的磁场分量会不断减小，从而导致较弱的磁共振。而对于TM模式，入射面上始终保持稳定的磁场分量，因此吸波能力随着入射角度的增大表现比较稳定。

为进一步分析该兼容隐身结构的吸波机理，通过CST电磁仿真软件监视了两个吸收峰（18.7 GHz和30.5 GHz）处的表面电流分布情况，如图4。通过观察可以看出在两个频点处发生强烈谐振的均为中间小正方形贴片以及四周四个大正方形，但不同的是在低频点（18.7 GHz）处，表面电流从上方单元经中间的小正方形贴片后流向下方单元，即形成单元间耦合；而在高频点（30.5 GHz）处，表面电流经中间小正方形在上下两组大正方形之间流动，即形成单元内耦合。

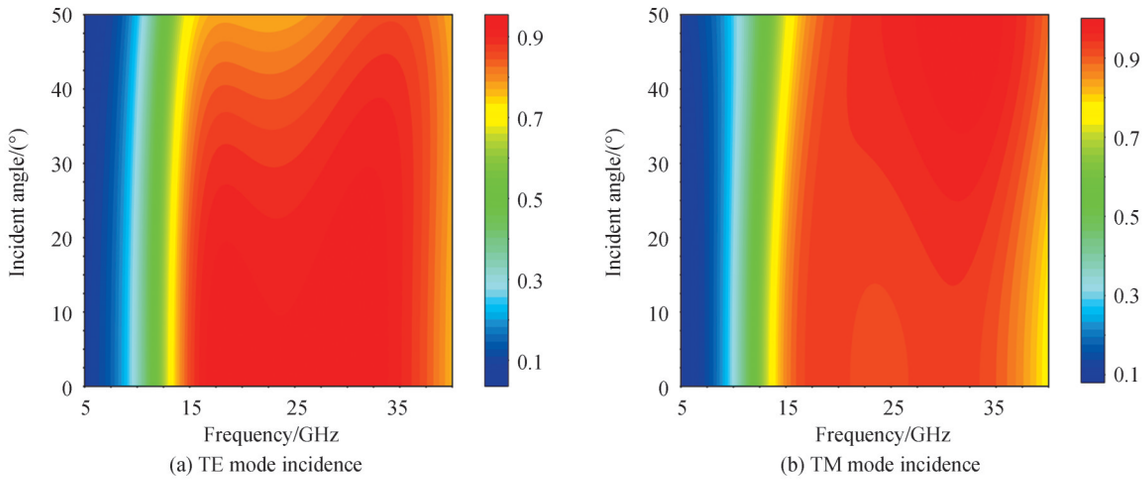

图3 不同入射角的吸收率仿真结果

Fig.3 Absorption simulation results of different incident angles

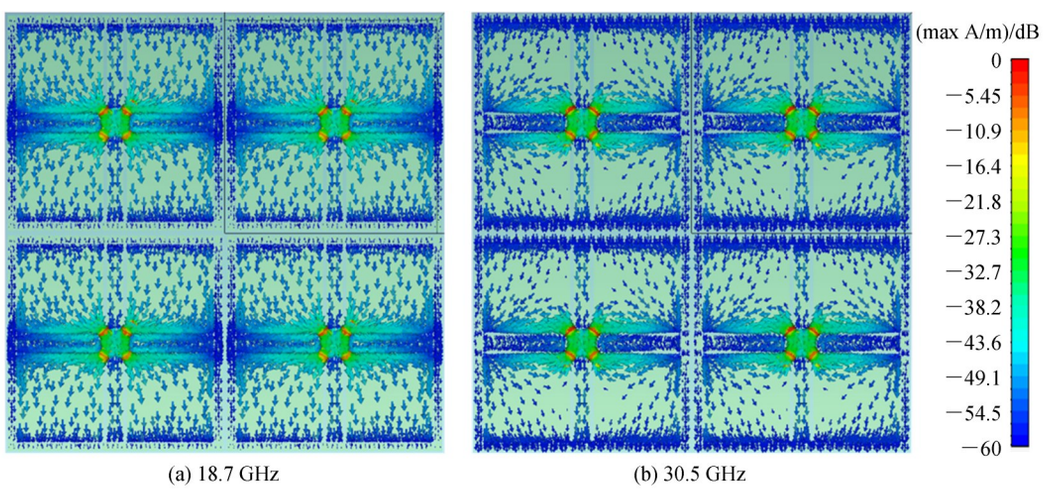

图4 两个吸收峰处表面电流分布情况

Fig. 4 Surface current distribution at the two absorption peaks

通过表面电流的分析，发现形成谐振结构的几乎只有中间小正方形贴片和四周四个大正方形贴片，而四个长方形贴片以及外围正方形贴片对于谐振消耗的贡献很小。图5考察了在没有四个长方形贴片以及外围正方形贴片的情况下，整体结构的吸收率。从图中可以看到，中间长方形贴片和外围正方形贴片对整体结构吸收率的影响主要集中在高频部分，当中间长方形贴片不存在时高频部分90%吸收的带宽能够提高将

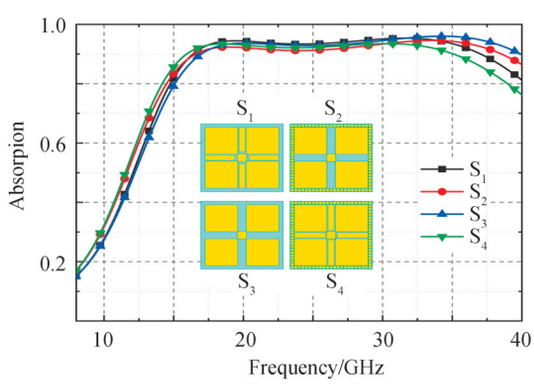

图5 不同表面结构的吸收率曲线

Fig.5 Absorption rate curves of different surface structures

近5 GHz，但这也意味着结构表面ITO占比的降低，进而影响了整体结构的红外发射率。经过计算，S_3单元结构表面ITO占比为63%，此时计算出红外发射率约为0.4，相比于S_4单元结构0.25的红外发射率有着较大幅度的上升。综合红外低发射和微波高吸收的要求，最终选择了如S_4所示的单元结构。

2 实验及讨论

2.1 样品加工及微波吸收性能

为进一步验证上述仿真结果，通过激光蚀刻技术将沉积在光学透明PET基板上的导电ITO膜蚀刻成设计的结构，如图6。图6(a)展示了所加工的样品，尺寸为360 mm×360 mm。图6(b)为表面结构细节图。

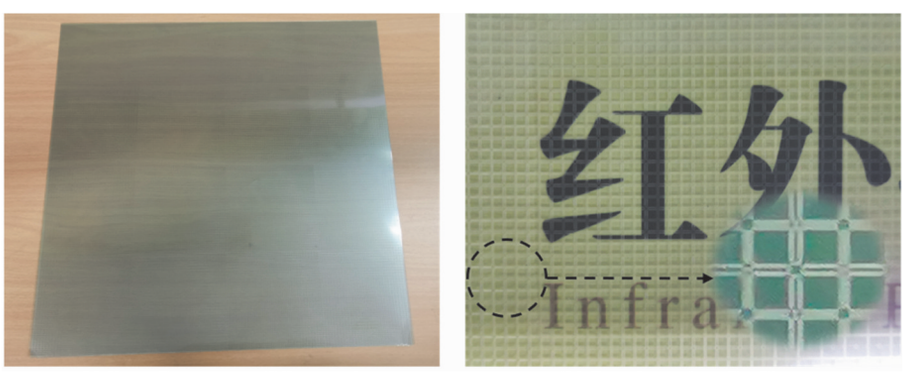

(a) Overall structure of the sample　　(b) Sample surface details

图6 光学透明红外-雷达兼容隐身超材料样品

Fig.6 Optical transparent infrared radar compatible stealth metamaterial sample

该红外-雷达兼容隐身结构在微波段的吸波性能在微波暗室中完成测试。测量系统由安捷伦N5224A网络分析仪和三对宽频带喇叭天线组成，如图7(a)，喇叭的工作频段分别为12.4～18.0 GHz、18.0～22.4 GHz以及22.4～40.0 GHz。每对喇叭天线其中一个充当电磁波发射器，另一个充当电磁波接受器，可测量反射率。测量时，首先选用相同尺寸的金属底板进行归一化，然后对反射率进行测量，经过计算后的吸收率曲线如图7(b)，其中实线为仿真结果，虚线为测量结果。考虑到样品加工中ITO的方阻以及尺寸可能存在误差，认为实验与仿真结果基本吻合。

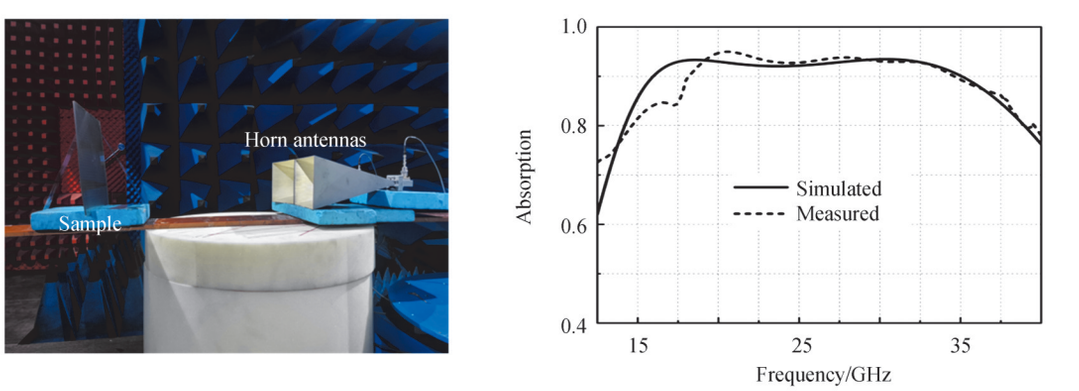

(a) Microwave test device　　(b) Comparison of experimental results and simulation results

图7 微波测试装置既实验结果

Fig. 7 Experimental results of microwave test device

2.2 光学透明特性和红外隐身性能

图6(b)展示了该结构的光学透明特性，为了精确表征其光学透明性能，使用紫外-可见光分光光度计(型号：UV-3600 plus)测量了整体结构的可见光透射率，结果如图8。经过计算，整体结构可见光平均透过率约为0.704，该结果有效地说明了所设计的一体化红外-雷达兼容隐身复合超表面在可见光波段具有较好的光学透明性能。

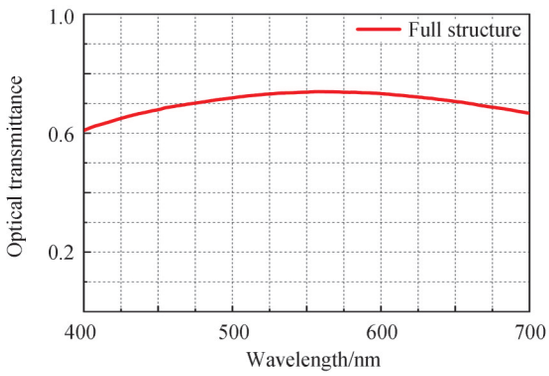

图8 可见光透过率测试结果

Fig. 8 Experimental results of optical transmittances

针对所设计结构的红外发射率，分别采用TSS-5X红外发射率测试仪（光谱响应范围：2～22 μm）和FTIR光谱仪对样品的发射率进行测量。利用TSS-5X红外发射率测试仪分别对6.0 Ω/sq的ITO薄膜、PET基底以及蚀刻了ITO图案的材料样品进行测量，为了保证测量数据的有效性，每种材料都选取五个不同位置进行测量，测量结果如表1。将所测得ITO薄膜和PET的发射率带入式(2)中，求得发射率为0.246，这与测量得到的所设计材料样品红外发射率平均值0.248十分接近。

表1 TSS-5X红外发射率测试仪测量结果

Table 1 Measurement results of TSS-5X infrared emissivity tester

Material	Infrared emissivity at different measured locations					The average
	Position 1	Position 2	Position 3	Position 4	Position 5	
ITO 6.0 Ω/sq	0.12	0.12	0.12	0.13	0.12	0.122
PET	0.90	0.90	0.90	0.89	0.89	0.896
Sample	0.24	0.25	0.24	0.26	0.25	0.248

进一步，利用FTIR光谱仪测量得到了3.0～14.0 μm波段范围内所设计结构的样品的红外发射率，结果如图9。可以看到光谱范围内发射率在0.25左右，计算波段范围内的平均发射率为0.255，与理论计算值和TSS-5X红外发射率测试仪所得到的测量值都比较接近，可以认为所设计的结构具有比较好的红外隐身能力。

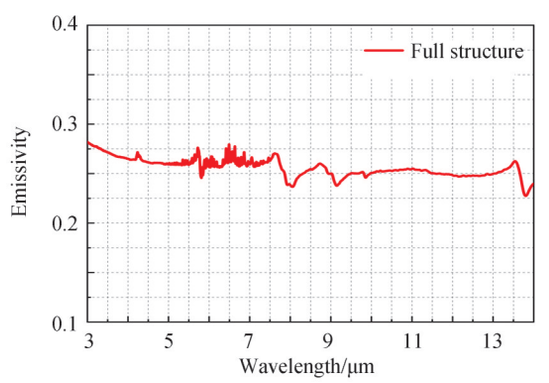

图9 FTIR光谱仪测量对红外发射率的测量结果

Fig. 9 Result of infrared emissivity measurement by FTIR spectromete

3 结论

基于可见光透明材料氧化铟锡（ITO）、聚对苯二甲酸乙二醇酯（PET）以及聚甲基丙烯酸甲酯（PMMA），设计并实现了一体化的可见光透明红外-雷达兼容隐身复合超表面。通过提高雷达吸波层表面

ITO占空比的方法,在保证雷达吸波性能的前提下降低了红外波段3.0～14.0 μm的发射率,实现了微波波段15.9～35.1 GHz频带范围内高于90%的宽带吸波以及红外波段0.25左右的低发射率,同时具有可见光透过率高、厚度薄的特点,在多光谱隐身领域具有很大实际应用价值。

参考文献

[1] TIAN Hao, LIU Haitao, CHENG Haifeng. A thin radar-infrared stealth-compatible structure: design, fabrication, and characterization[J]. Chinese Physics B, 2014, 23(2): 025201.

[2] PAN X Y, WANG X J, WANG R X, et al. Infrared radiation and stealth characteristics prediction for supersonic aircraft with uncertainty[J]. Infrared Physics & Technology, 2015, 73: 238-250.

[3] PANG Y Q, LI Y F, YAN M B, et al. Hybrid metasurfaces for microwave reflection and infrared emission reduction[J]. Optics Express, 2018, 26(9): 11950-11958.

[4] ZHONG S M, WU L J, LIU T J, et al. Transparent transmission-selective radar-infrared bi-stealth structure[J]. Optics Express, 2018, 26(13): 16466-16476.

[5] YE Shengtian, LIU Chaohui, CHENG Shengyue, et al. Research progress of infrared stealth materials at home and abroad [J]. Laser and Infrared, 2015, 45(11): 1285-1291.
叶圣天,刘朝辉,成声月,等.国内外红外隐身材料研究进展[J].激光与红外,2015,45(11):1285-1291.

[6] KLUSKENS M S, NEWMAN E H. Scattering by a chiral cylinder of arbitrary cross section[J]. IEEE Transactions on Antennas and Propagation, 1990, 38(9): 1448-1455.

[7] ZHANG J K, LIU R H, ZHAO D P, et al. Design, fabrication and characterization of a thin infrared-visible bi-stealth film based on one-dimensional photonic crystal[J].Optical Materials Express, 2019, 9(1): 195-202.

[8] WANG Y, CHENG H F, WANG J, et al. Infrared emissivity of capacitive frequency-selective surfaces and its application in radar and IR compatible stealth sandwich structures[J].Advanced Materials Research, 2012, 382: 65-69.

[9] CAO Xiaoli, GE Hongying, XING Honglong, et al. Preparation and performance of MWCNTs/ZnO radar-infraredcompatible stealth materia[J].Journal of Fuyang Normal University(Natural Science Edition), 2015 ,32(2): 46 -50.
曹小丽,葛红影,邢宏龙,等. MWCNTs /ZnO雷达-红外兼容隐身材料的制备及性能研究[J].阜阳师范学院学报(自然科学版),2015,32(2):46-50.

[10] MA Chengyong, CHENG Haifeng, TANG Gengping, et al. Research progress of infrared/radar compatible stealth materials[J]. Materials Reports, 2007, 21(1): 126-132.
马成勇,程海峰,唐耿平,等.红外/雷达兼容隐身材料的研究进展[J].材料导报,2007,21(1):126-132.

[11] CHEN Yanpeng, XU Guoyue, GUO Tengchao, et al. Application of modified carbonyl iron powder in infrared/radar compatible coatings[J]. Ordnance Material Science and Engineering, 2010, 33(5): 42-45.
陈砚朋,徐国跃,郭腾超,等.改性羰基铁粉在红外/雷达兼容涂层中的应用[J].兵器材料科学与工程,2010,33(5):42-45.

[12] GAO Yongfang, SHI Jiaming, ZHAO Dapeng, et al. Design and fabrication of a kind of far infrared and 10.6μm laser band compatible camouflage material based on photonic crystals[J]. Acta Optica Sinica, 2011, 31(6): 155-158.
高永芳,时家明,赵大鹏,等.一种基于光子晶体的远红外与10.6μm激光兼容伪装材料的设计与制备[J].光学学报,2011,31(6):155-158.

[13] ZHANG Z Y, XU M Z, RUAN X F, et al. Enhanced radar and infrared compatible stealth properties in hierarchical SnO2@ZnO nanostructures[J]. Ceramics International, 2017, 43(3): 3443-3447

[14] QI D, CHENG Y, WANG X, et al. Multi-layer composite structure covered polytetrafluoroethylene for visible-infrared-radar spectral compatibility[J]. Journal of Physics D Applied Physics, 2017, 50(50): 505108.

[15] QI D, WANG X, CHENG Y, et al. Design and characterization of one-dimensional photonic crystals based on ZnS/Ge for infrared-visible compatible stealth applications[J]. Optical Materials, 2016, 62: 52-56.

[16] ZHANG C, YANG J, YUAN W, et al. An ultralight and thin metasurface for radar-infrared bi-stealth applications[J]. Journal of Physics D Applied Physics, 2017, 50(44): 444002.

[17] XU C, WANG B, PANG Y, et al. Hybrid metasurfaces for infrared-multiband radar stealth-compatible materials applications[J]. IEEE Access, 2019, 7: 147586-147595.

[18] SHRESTHA S, WANG Y, OVERVIG A ,et al. Indium tin oxide broadband metasurface absorber[J]. ACS Photonics, 2018, 5(9): 3526-3533.

[19] ZHANG C, CHENG Q, YANG J, et al. Broadband metamaterial for optical transparency and microwave absorption[J]. Applied Physics Letters, 2017, 110(14): 143511.

[20] MENG Z, TIAN C, XU C, et al. Multi-spectral functional metasurface simultaneously with visible transparency, low infrared emissivity and wideband microwave absorption[J]. Infrared Physics & Technology, 2020, 110: 103469.

[21] XU Cuilian, MENG Yueyu, WANG Jiafu, et al. Optically transparent hybrid metasurfaces for low infrared emission and wideband microwave absorption[J]. Acta Photonica Sinica, 2021, 50(4): 0416001.

徐翠莲,孟跃宇,王甲富,等.光学透明红外与雷达兼容隐身复合超表面[J].光子学报,2021,50(4):161-170.
[22] YANG J F, XU C L, QU S B, et al. Optical transparent infrared high absorption metamaterial absorbers[J]. Journal of Advanced Dielectrics,2018,8(1):1-8.
[23] ZHONG S M, JIANG W, XU P P, et al. A radar-infrared bi-stealth structure based on metasurfaces[J]. Applied Physics Letters,2017,110(6):063502.

Integrated Design of Optically Transparent Composite for Low Infrared Emission and Wideband Microwave Absorption Metasurface

XIAO Tong, TIAN Changhui, XU Cuilian, GAO Zhiqiang
(*Department of Basic Science, Air Force Engineering University, Xi'an* 710051, *China*)

Abstract: In recent years, metamaterials have attracted great attention in stealth technology. As a special two-dimensional metamaterial, hypersurface is more suitable for the design of infrared radar compatible stealth structures. Based on optically transparent materials Indium Tin Oxide (ITO), Polyethylene Terephthalate (PET) and Polymethyl Methacrylate (PMMA), an optically transparent infrared radar compatible stealth composite metasurface is realized by using the idea of integrated design of infrared low emission layer and radar absorbing layer. The structure consists of three parts: functional layer, dielectric layer, and reflective back plate, with a total thickness of only 1.17 mm. By etching the ITO pattern on the surface of the functional layer and optimizing the pattern size of the pattern, the broadband absorption higher than 90% in the frequency range of 15.9~35.1 GHz in the microwave band is realized. At the same time, the infrared emissivity is reduced by increasing the ITO duty cycle on the surface of the functional layer, and the infrared emissivity on the surface of the structure is controlled at 0.25. Based on the analysis of the surface current of the material, the mechanism of super surface absorbing wave is expounded, and the influence of different patches on the absorbing wave ability is analyzed. Through the analysis of surface current, it is found that almost only the small square patch in the middle and four large square patches around form the resonant structure, while the four rectangular patches and the peripheral square patches make little contribution to the resonant consumption. When the middle rectangular patch does not exist, the bandwidth absorbed by 90% of the high frequency part can be increased by nearly 5 GHz, but it also means that the proportion of ITO on the surface of the structure is reduced, which affects the infrared emissivity of the whole structure. Through simulation experiments, the changes of the absorbing capacity of the designed structure at different incident angles are discussed. For TE mode, the structure can maintain high absorptivity when the incident angle is less than 30°. With the further increase of the angle, the absorptivity of the low-frequency part decreases more. For TM mode, the absorptivity of the structure is only about 0.8 when the incident angle is small. With the increase of the incident angle to 35°, the structure can maintain 90% absorptivity in the range of 20.1~35.0 GHz. It shows that the absorbing ability of the structure at large incident angle in TM mode is stronger than that in TE mode. In order to further verify the simulation results, the conductive ITO film deposited on the optically transparent PET substrate was etched into the designed structure by laser etching technology, and the experimental sample was processed, the sample size was 360 mm×360 mm. The microwave absorption capacity, infrared emissivity and visible light transmittance of the sample were measured respectively. The microwave absorption performance is tested in the microwave darkroom. The measurement system is composed of Agilent N5224a network analyzer and three pairs of broadband horn antennas. During the measurement, the metal base plate with the same size is selected for normalization, and then the reflectivity is measured. After calculation, the absorption curve is obtained. Considering the square resistance and size error of ITO in sample processing, it is considered that the experimental results are basically consistent with the simulation results. The optical transparency performance is measured by ultraviolet visible spectrophotometer (model: uv-3600 plus). After calculation, the average visible light transmittance of the overall structure is about 0.704. The results effectively show that the designed integrated infrared radar compatible stealth composite hypersurface has good optical transparency performance in the visible band. For the infrared emissivity of the designed structure, Tss-5x infrared emissivity tester (spectral response range: 2~22 μm) and FTIR spectrometer

are used to measure the emissivity of the sample. ITO film of 6.0 Ω/sq, pet substrate and material samples etched with ITO pattern are measured respectively. In order to ensure the effectiveness of the measured data, each material is measured at five different positions, and the obtained infrared emissivity is 0.246, which is very close to the average infrared emissivity of the designed material sample obtained by direct measurement of 0.248. The infrared emissivity of the sample with the designed structure in the range of 3.0~14.0 μm is measured by FTIR spectrometer, which is about 0.25, which is close to the theoretical calculation value and the measurement value obtained by Tss-5x infrared emissivity tester. It can be considered that the designed structure has better infrared stealth ability. The structure has thin thickness, good broadband radar absorption performance, low infrared emissivity and visible light transparency.

Key words: Infrared-radar compatible stealth; Low infrared emissivity; Radar wave absorption; Metasurface; Optically transparent

OCIS Codes: 230.0040; 240.6700; 280.3640

Foundation item: National Natural Science Foundation of China (No. 12004437), Natural Science Basic Research Program of Shaanxi Province (No.2020JQ-471)